



Micromechanics-based complex modulus prediction of crumb rubber modified bitumen considering interparticle interactions

Haopeng Wang, Hong Zhang, Xueyan Liu, Athanasios Skarpas, Sandra Erkens & Zhen Leng

To cite this article: Haopeng Wang, Hong Zhang, Xueyan Liu, Athanasios Skarpas, Sandra Erkens & Zhen Leng (2021) Micromechanics-based complex modulus prediction of crumb rubber modified bitumen considering interparticle interactions, Road Materials and Pavement Design, 22:sup1, S251-S268, DOI: [10.1080/14680629.2021.1899965](https://doi.org/10.1080/14680629.2021.1899965)

To link to this article: <https://doi.org/10.1080/14680629.2021.1899965>



© 2021 The Author(s). Published by Informa UK Limited, trading as Taylor & Francis Group



Published online: 25 Mar 2021.



Submit your article to this journal [↗](#)



Article views: 340







View related articles [↗](#)



View Crossmark data [↗](#)

Micromechanics-based complex modulus prediction of crumb rubber modified bitumen considering interparticle interactions

Haopeng Wang ^{a,c}, Hong Zhang^a, Xueyan Liu^a, Athanasios Skarpas ^{a,b},
Sandra Erkens ^a and Zhen Leng ^c

^aSection of Pavement Engineering, Faculty of Civil Engineering & Geosciences, Delft University of Technology, Delft, The Netherlands; ^bDepartment of Civil Infrastructure and Environmental Engineering, Khalifa University, Abu Dhabi, United Arab Emirates; ^cDepartment of Civil and Environmental Engineering, The Hong Kong Polytechnic University, Hong Kong, People's Republic of China

ABSTRACT

Crumb rubber modified bitumen (CRMB) can be regarded as a binary composite system in which swollen rubber particles are embedded in the bitumen matrix. The current study aims to further improve the prediction accuracy of micromechanical models for CRMB by considering the interparticle interactions. To accomplish this goal, two different strategies were used. Firstly, the (n+1)-phase model was applied to the CRMB system by considering the multilayer properties of swollen rubber particles. Secondly, a new micromechanical scheme called the J-C model was used to account for the interparticle interaction issue. Results show that the (n+1)-phase models slightly increase the prediction accuracy but the underestimation of complex modulus at lower frequencies remains unsolved. The J-C model remedies the underestimation of modulus in the low-frequency range by other models and provides an overall improvement for the relative prediction accuracy by properly addressing the interparticle interactions from the perspective of particle configuration.

ARTICLE HISTORY

Received 10 July 2020
Accepted 2 March 2021

KEYWORDS

Crumb rubber modified bitumen; micromechanics; complex shear modulus; interparticle interaction; radial distribution function

1. Introduction

Millions of tons of end-of-life tires are produced every year worldwide. The incorporation of crumb rubber from ELTs into bitumen not only provides a solution for the disposal of scrap tyres but also enhances the performance of Hot-Mixed Asphalt (HMA) mixes by increasing the resistance of pavements to permanent deformation, thermal and fatigue cracking (Nanjegowda & Biligiri, 2020). The superior performance of rubberised asphalt mixtures is mainly attributed to the interaction between bitumen and rubber. Depending on different mixing temperature, time and rate, etc., bitumen-rubber interaction generally consists of two mechanisms: (i) rubber swelling in bitumen matrix due to the absorption of the light fractions of bitumen; and (ii) rubber degradation through chain disentanglement and chain scission reactions (Wang, Apostolidis, et al., 2020). The raw material parameters (e.g. the nature of bitumen and rubber) (Willis et al., 2013) were also reported to significantly influence the interaction process of rubber in bitumen and hence the physical and mechanical properties of crumb rubber modified bitumen (CRMB).

A thorough understanding of the interaction conditions and raw material characteristics will guide the material selection and process optimisation to obtain desired binder properties from the modification. One of the vital questions needs to be answered is how to effectively predict the properties of

CONTACT Haopeng Wang  haopeng.wang@tudelft.nl

modified binders instead of carrying out tedious laboratory work. Numerical and analytical models are often used to accomplish this goal. Although substantial work has been done to characterise and even predict empirical and fundamental properties of CRMB, scarce work has been reported to investigate the complicated behaviours of CRMB using rigorous mechanics-based models (Medina & Underwood, 2017; Wang, Liu, Zhang, Apostolidis, Erkens, et al., 2020). A few empirical models were developed to correlate rubber characteristics (particle size, surface area, etc.) to resultant CRMB responses (Shen et al., 2009a; 2009b). These straightforward models are incapable of providing theoretical insights into the impact of multi-physical interactions between the constituents.

By contrast, micromechanical models deduced by the homogenisation process can predict fundamental material properties of a composite based on properties and volume fractions of individual constituents (Charalambakis, 2010). Numerical micromechanical models, i.e. finite element models (FEM) and discrete element models (DEM), have been developed by many researchers (Aragao et al., 2011; Caro et al., 2010; Leon L. Mishnaevsky & Schmauder, 2001; Sadd et al., 2004) to predict the properties of a mix with complex compositions. However, these studies also highlighted that FEM/DEM-meshes with detailed information (usually by means of X-ray CT scan) require large-scale computational facilities, which limits the utilisation of such models in practice. Alternatively, analytical micromechanical models are expected to provide reliable predictions of the mechanical properties of a composite without extensive computational efforts. Analytical micromechanical models developed based on continuum mechanics have increasingly been used to predict the effective mechanical properties of bituminous materials (Yin et al., 2008; Zhang et al., 2020).

For asphalt mastic or mixture system, fillers and aggregates are usually regarded as inert rigid materials embedded in the bitumen matrix (Buttlar et al., 1999; Shu & Huang, 2008). The CRMB composite can be regarded as a binary system in which bitumen is the matrix while rubber particles are the inclusions. Unlike asphalt mastic or mixture system, the composite system of CRMB is more sophisticated due to the bitumen-rubber interaction which changes both the mechanical properties and volume fractions of individual constituents (Wang et al., 2020). The stiffening or reinforcement mechanisms of rubber in bitumen mainly include volume-filling reinforcement, physiochemical interaction and inter-particle interaction (Wang, Liu, Zhang, Apostolidis, Erkens, et al., 2020). How to properly address these reinforcement mechanisms of CRMB using micromechanical modelling remains a challenge.

Practically speaking, if it is applicable to accurately predict the mechanical properties of CRMB from the known properties and blend percentages of the constituent phases by using micromechanical models, it can save the time and cost for the tedious laboratory work, which enables a more appropriate design of binders (determination of bitumen and rubber type, rubber content and particle gradation) and enhanced material development (binder preparation conditions).

2. Micromechanics-based analysis of CRMB

To estimate the effective properties of a heterogeneous composite based on the microstructural description and the local behaviours of its constituents, homogenisation theory was developed to derive a homogenised description for the medium based on the assumption of representative volume element (RVE) (Charalambakis, 2010). As stated before, CRMB can be regarded as a binary system with rubber as the inclusion and bitumen as the matrix. Figure 1 schematically illustrates the RVE of the CRMB composite system before and after bitumen-rubber interaction. After the potential physiochemical interaction, the properties of both bitumen and rubber phases have significantly changed. In general, bitumen-rubber interaction has four impacts from a micromechanics-based point of view: (1) changing the component compositions and thus the mechanical properties of bitumen matrix due to the absorption of light fractions by rubber and the potential released components from rubber; (2) changing the mechanical properties of rubber due to the formation of a gel-like structure after swelling; (3) changing the volume content of rubber due to swelling (the so-called effective volume fraction); (4) changing the interfacial properties between bitumen and rubber due to aforementioned factors (Wang, Liu, Zhang, Apostolidis, Scarpas, et al., 2020). Therefore, the accurate determination

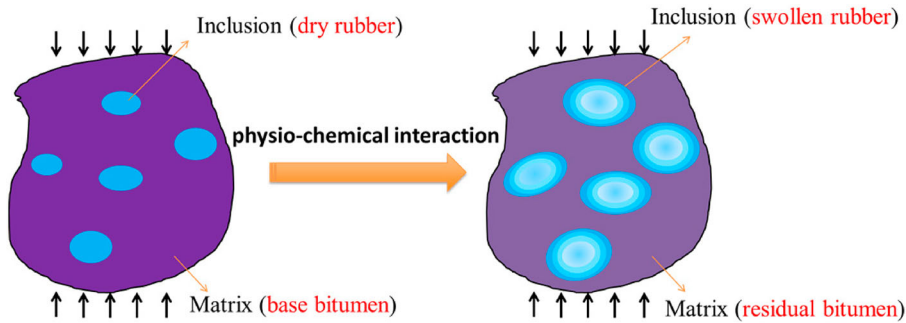


Figure 1. Schematic representation of the RVE of the CRMB composite system before and after interaction.

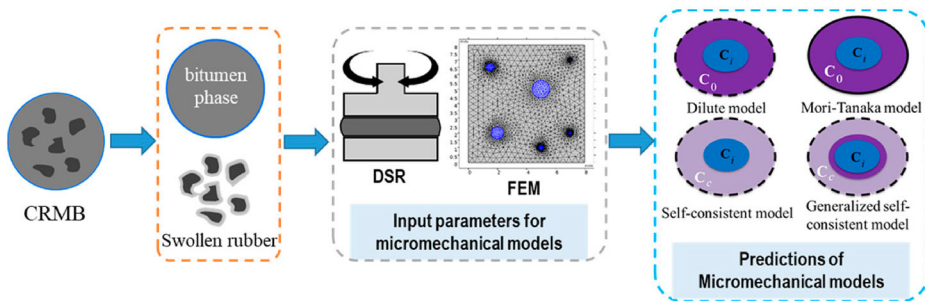


Figure 2. Laboratory tests and numerical tools to obtain the input constituent parameters for micromechanical models.

of input parameters from constituents, as a challenge, directly influence the level of accuracy of the model prediction.

A previous study (Wang, Liu, Zhang, Apostolidis, Erkens, et al., 2020) has developed dedicated laboratory tests and numerical tools to obtain the input constituent parameters for micromechanical models as shown in Figure 2. The bitumen matrix, which is the liquid phase of CRMB after removing the insoluble rubber particles, was tested by a dynamic shear rheometer (DSR) to obtain the rheological properties. DSR measurements were also carried out on the prepared swollen rubber samples to obtain the mechanical properties of rubber after swelling in bitumen (Wang, Liu, Apostolidis, et al., 2020). The effective volume fraction of rubber after swelling was determined by the finite element method (FEM). A finite element model capable of simulating the multiphysics swelling phenomenon (mass diffusion and volume expansion) was developed previously (Wang et al., 2019). After determining the necessary input parameters, they were implemented into four typical micromechanical models, i.e. the dilute model (DM), the Mori-Tanaka model (MTM), the self-consistent model (SCM), the generalised self-consistent model (GSCM), to predict the complex modulus of CRMB. The predicted results were then compared with the experimental data.

It was found that four common micromechanical models are applicable for predicting the complex shear modulus of CRMB with various rubber contents. Figure 3 presents the comparison between different micromechanical models for predicting the complex modulus of CRMB-22 (i.e. rubber content is 22% by weight of base bitumen) as an example. The data of complex moduli were plot in a form of master curves at a reference temperature of 30 °C in Figure 3. To quantitatively compare the model prediction accuracy, the goodness-of-fit statistics (S_e/S_y and R^2) shown in the figure were calculated with reference to the line of equality using Equations (1) to (3) (Ceylan et al., 2009).

$$S_y = \sqrt{\frac{\sum_{i=1}^n (G_{mi}^* - \bar{G}_m^*)^2}{n}} \quad (1)$$

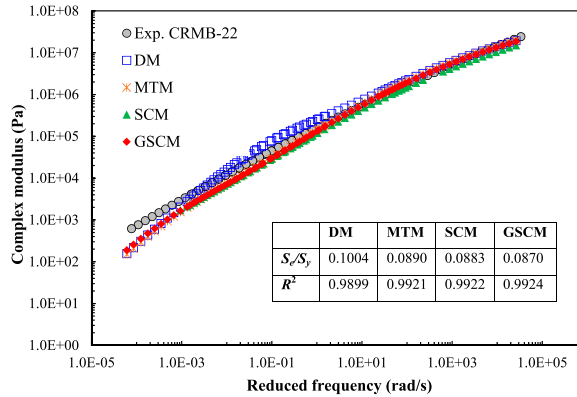


Figure 3. Comparison of different micromechanical models for predicting the complex modulus.

$$S_e = \sqrt{\frac{\sum_{i=1}^n (G_{pi}^* - \overline{G_m^*})^2}{n - k}} \quad (2)$$

$$R^2 = 1 - \frac{n - k}{n - 1} \left(\frac{S_e}{S_y} \right)^2 \quad (3)$$

where n is the number of data points; k is the number of independent variables in the model; G_{mi}^* is the measured complex modulus; $\overline{G_m^*}$ is mean value of measured complex modulus; G_{pi}^* is the model predicted complex modulus; S_y is the standard deviation of the measured complex modulus; S_e is the standard error; R^2 is the coefficient of determination. S_e/S_y is the relative prediction error.

It can be found that MTM, SCM, and GSCM provide similar predictions but GSCM has the highest prediction accuracy as indicated by the lowest relative error ($S_e/S_y = 0.0870$) and the highest coefficient of determination ($R^2 = 0.9924$). All the micromechanical models give reasonable predictions at low rubber contents while yielding biased predictions at low frequencies range with high rubber contents. Considering that the low-frequency range corresponds to the high-temperature range in the frame of master curves, rubber particle interaction will be more prominent in CRMB at high temperatures since the bitumen phase is softer. The underestimation of complex modulus at high temperatures is because these models were primarily developed to address the stiffening effect resulting from the embedded inclusions in a matrix with minimal or limited particle interactions. which is the case of dispersed suspensions (Yin et al., 2008; Zhang et al., 2018). Under this circumstance, the mechanical behaviour of the suspension is dominated by the matrix phase. While at high temperatures, for the case of CRMB, the rubber inclusion may have more dominant effects on the binder mechanical behaviours than the bitumen matrix does. Therefore, to amend the underestimation of the complex modulus of CRMB in the low-frequency range, the interparticle interactions need to be further addressed.

The aim of the current study is to further improve the prediction accuracy of micromechanical models for CRMB by considering the interparticle interactions. To accomplish this goal, two different strategies were used. Firstly, the $(n+1)$ -phase model was applied to the CRMB system by considering the multilayer properties of swollen rubber particles. Secondly, a new micromechanical scheme called the J-C model was used to account for the interparticle interaction issue. To this end, approximate solutions for the pairwise particle interaction problem were proposed with the help of the conditional probability function (mainly the radial distribution function).

3. Determination of input constituent parameters for micromechanical models

3.1. Materials and methods

Penetration grade 70/10 bitumen (Nynas) and crumb rubber from waste truck tires (Kargro) using ambient grounding process were used to prepare the CRMB binders. The crumb rubber particles have

a size ranging from 0 to 0.71 mm. Detailed technical information about bitumen and crumb rubber can be found in (Wang, Liu, Zhang, Apostolidis, Erkens, et al., 2020). High-shear mixer in the laboratory was used to prepare CRMB binders by blending different percentages of crumb rubber with base bitumen at 180 °C for 30 min according to the optimised mixing procedure (Wang, Liu, Zhang, Apostolidis, Scarpas, et al., 2020). To more efficiently address the issue of underestimation of complex modulus at lower frequencies, only binder CRMB-22 (i.e. rubber content is 22% by weight of base bitumen) was investigated in the current study since the interparticle interaction effects are more prominent at high rubber contents.

To effectively predict the mechanical properties of CRMB with micromechanical models, the mechanical properties of both bitumen matrix and rubber inclusion are required. In addition, the volume fraction of each phase also needs to be determined. Since the nature of both bitumen and rubber phases have changed after the interaction, it is of great importance to measure the representative rheological properties of actual bitumen matrix and rubber inclusion as well as the effective volume fraction of rubber after swelling in the CRMB system. Dedicated laboratory tests and numerical simulations were performed to obtain these input parameters as shown in Figure 2 (Wang, Liu, Zhang, Apostolidis, Erkens, et al., 2020). The bitumen matrix was extracted by filtering the insoluble rubber particles from CRMB with a mesh sieve (0.063-mm) at 163°C. Cylindrical rubber samples (2-mm in thickness and 8-mm in diameter) were cut from waste truck tire tread using the water jet cutting technology. These dry rubber samples were soaked in hot bitumen at 180°C for 36 h to prepare the swollen rubber samples to represent the rubber particle phase in CRMB. The Poisson's ratios of the bitumen phase and rubber phase were assumed to be 0.49 and 0.45, respectively (Aurangzeb et al., 2016). The detailed information on sample preparation and laboratory test are omitted here and only the results are reported.

3.2. Rheological properties of bitumen phase and rubber phase

A modified Christensen-Anderson-Marasteanu (CAM) model together with the Williams-Landel-Ferry (WLF) equation were used to generate binder master curves of complex modulus and phase angle based on the frequency sweep test data (Wang et al., 2018). By contrast, a generalised logistic function was used for establishing the master curves for swollen rubber samples since rubber is not a rheologically simple material, which common rheological models for bitumen are not suitable for (Wang, Liu, Apostolidis, et al., 2020). Figure 4 presents the complex modulus and phase angle master curves of base bitumen and the liquid phase (bitumen matrix) at a reference temperature of 30 °C. The liquid phase of CRMB-22 (CRMB-22-LP) is stiffer and more elastic than the base bitumen as indicated by the increased complex modulus and decreased phase angle. This is because the light fractions of bitumen (mainly aromatic oils) were absorbed by crumb rubber during the interaction process. This in turn increases the proportions of asphaltenes which primarily contributes to the increase of stiffness and elasticity in bitumen.

Figure 5 plots the rheological master curves of dry and swollen rubber samples at a reference temperature of 30 °C. It is noteworthy that dry rubber exhibits obvious elastic behaviours whose complex modulus and phase angle are almost frequency independent, while the swollen rubber exhibits obvious viscoelasticity. After the swelling process, the swollen rubber sample became softer and more viscous than the dry rubber due to the absorption of bitumen components, forming a gel-like structure.

3.3. Effective volume content of rubber in CRMB

The effective volume content of rubber in CRMB was estimated by the developed finite element model in conjunction with the crumb rubber gradation. The densities of bitumen and crumb rubber used for estimating the effective volume content of rubber in CRMB were 1.03 and 1.15 g/cm³, respectively. The swelling ratios of rubber particles of different sizes after mixing were presented in Figure 6. The particle size in the figure represents the mean value of two consecutive sieve sizes. Small rubber particles reach

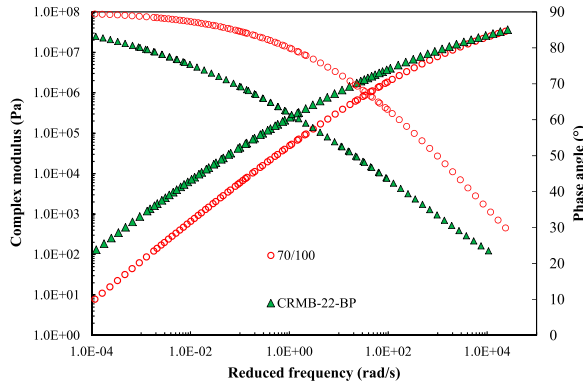


Figure 4. Complex modulus and phase angle master curves of bitumen matrices at the reference temperature of 30 °C.

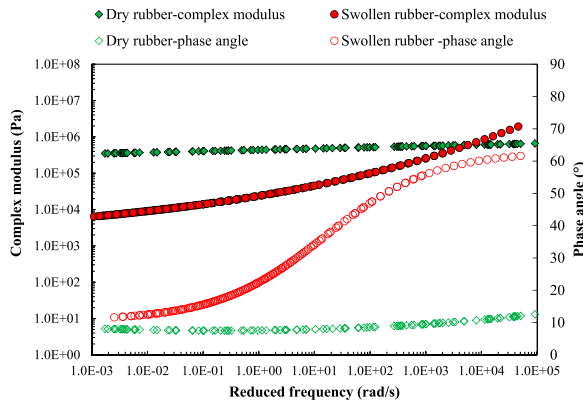


Figure 5. Complex modulus and phase angle master curves of rubber inclusions at the reference temperature of 30 °C.

the swelling equilibrium faster than large rubber particles. Under a prescribed interaction/mixing time, the swelling ratio of large rubber particles is lower than that of small rubber particles due to insufficient swelling. With the known crumb rubber gradation, the weighted averaged swelling ratio of rubber in CRMB is approximately 2.126. Based on the densities of bitumen and crumb rubber, the effective volume content of rubber in CRMB-22 was estimated as 35%. Till this, all the necessary input parameters for performing micromechanical analysis are determined.

4. Model modification based on GSCM

4.1. (n+1)-phase model

The GSC model was further generalised to the (n+1)-phase model by accounting for the inclusions coated with an indefinite number of layers (Figure 7). In the (n+1)-phase model, an n-layered spherical inclusion surrounded by the matrix material (phase n) is embedded in an infinite medium (Herve & Zaoui, 1993). Phase 1 with a radius of R_1 constitutes the central core while phase r lying within the shell is limited by the spheres with radii of R_{r-1} and R_r . The effective shear modulus of the composite using the (n+1)-phase model can also be solved by a quadratic equation as Equation (4).

$$A \left(\frac{G_c}{G_b} \right)^2 + B \left(\frac{G_c}{G_b} \right) + C = 0 \tag{4}$$

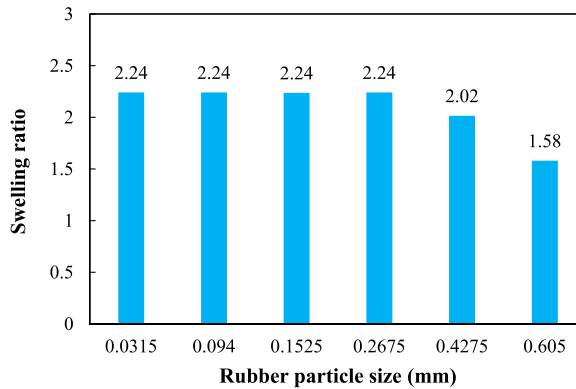


Figure 6. The swelling ratios of rubber particles of different sizes after mixing.

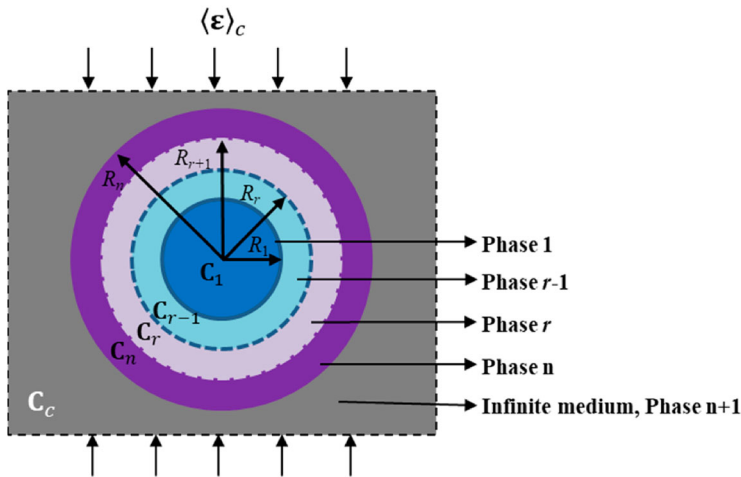


Figure 7. Schematic illustration for the $(n+1)$ -phase model.

where G_c and G_b are the shear modulus of the CRMB and the bitumen matrix, respectively. Coefficients A, B, and C are related to the mechanical properties (e.g. Poisson's ratio) and volume fraction of each phase. The detailed formulations of these parameters can be found in (Zhang et al., 2020).

The $(n+1)$ -phase model is frequently used when additional phases are required to be modelled between the inclusion and the matrix. For instance, the additional phase can be an actual coating material for the inclusion or the inclusion has a multilayered structure due to the physiochemical interactions between different phases. As demonstrated in a previous study, swelling of rubber particles in bitumen results in a multilayered structure of the swollen rubber particles before reaching the equilibrium state (Wang, Apostolidis, et al., 2020). Intuitively, the different layers with the rubber particles have different mechanical properties where the outer layer is softer than the inner layer due to the ingress of bitumen components. In the current model, phase n is the bitumen matrix while phase 1 to r are the multilayers of swollen rubber particles. Therefore, the $(n+1)$ -phase model may be a good alternative to model the mechanical behaviours of CRMB, which was tried in this study.

4.2. $(n+1)$ -phase model for the CRMB system

The schematic illustrations of the $(n+1)$ -phase model for the CRMB system are presented in Figure 8. Figure 8a shows the three-phase model (GSCM) in the context of CRMB, where the fully swollen rubber

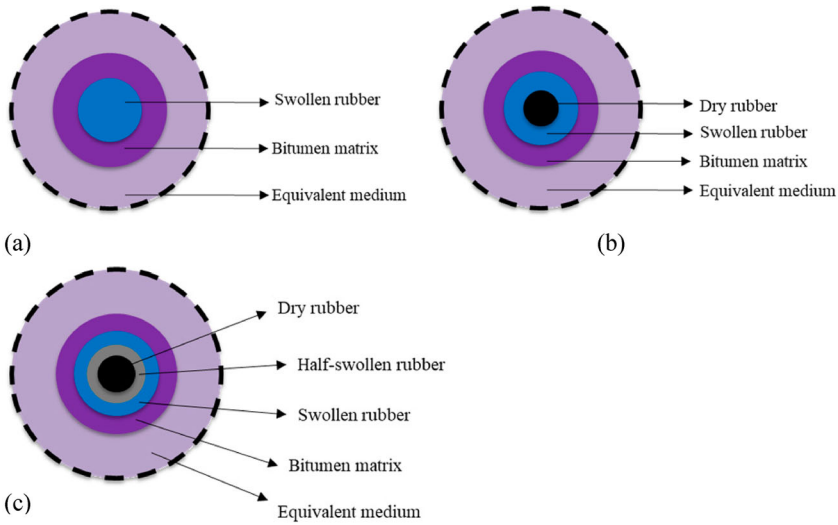


Figure 8. Schematic illustrations of the $(n+1)$ -phase model for CRMB system (a) 3-phase, GSCM; (b) 4-phase; (c) 5-phase.

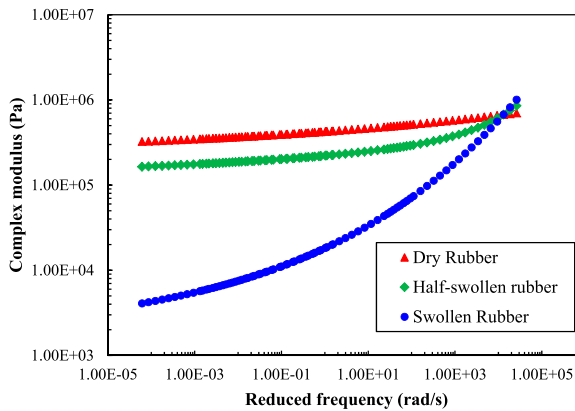


Figure 9. Complex modulus master curves of rubber inclusions at a reference temperature of 30 °C.

particles surrounded by the bitumen matrix are embedded in an infinite medium with the equivalent mechanical properties of CRMB. Figure 8b added an additional phase of dry rubber as the core to form the 4-phase model. This is because the inner cores of large rubber particles maybe not swollen after a limited mixing time. Figure 8c further divided the rubber particle into three layers: dry rubber, half-swollen rubber, fully swollen rubber. The mechanical properties of dry rubber and swollen rubber can be directly taken from Figure 5. The mechanical properties of half-swollen rubber were obtained by averaging the properties of dry rubber and swollen rubber.

4.2.1. Input parameters for the $(n+1)$ -phase model

Mechanical properties and volume fractions of individual constituents are required to perform the micromechanical analysis. For the $(n+1)$ -phase model, mechanical properties of bitumen matrix, dry rubber inclusion, swollen rubber inclusion were obtained by previous laboratory tests. The mechanical properties, particularly the complex modulus master curve, of half-swollen rubber was obtained by averaging the properties of dry rubber and swollen rubber as shown in Figure 9.

Table 1. Volume fraction of each phase for the 4-phase model.

| Volume fraction | Case 1 | Case 2 | Case 3 | Case 4 |
|-------------------------|--------|--------|--------|--------|
| Dry rubber V_{dr} | 5% | 10% | 15% | 20% |
| Swollen rubber V_{sr} | 30% | 25% | 20% | 15% |
| Bitumen matrix V_b | 65% | 65% | 65% | 65% |

Table 2. Volume fraction of each phase for the 5-phase model.

| Volume fraction | Case 1 | Case 2 | Case 3 | Case 4 |
|-------------------------------|--------|--------|--------|--------|
| Dry rubber V_{dr} | 15% | 10% | 5% | 5% |
| Half-swollen rubber V_{hsr} | 10% | 10% | 10% | 5% |
| Swollen rubber V_{sr} | 10% | 15% | 20% | 25% |
| Bitumen matrix V_b | 65% | 65% | 65% | 65% |

From the previous FE analysis, the effective volume contents of rubber in CRMB-22 is 35%. To properly apply the $(n+1)$ -phase model on the binder, it is crucial to have the volume fractions of different phases. Although it is possible to have an idea about to what extent each sized rubber particle has swelled by FE simulation, it is complicated to calculate the exact volume fractions of different layers of rubber because of the existence of swelling gradient from the surface layer to the inner core. Therefore, parametric analysis was performed by assuming several different volume fraction combinations of rubber inclusion. Tables 1 and 2 respectively shows the volume fraction of each phase used in the 4-phase model and 5-phase model.

4.2.2. Prediction results of the $(n+1)$ -phase model

With the available input parameters, a Matlab code was programmed to implement the complex equations in the $(n+1)$ -phase model to calculate the predicted results. The predicted complex modulus master curves at 30 °C for different cases are shown in Figure 10. From Figure 10(a), the predicted results using the 4-phase model yield slightly more accurate predictions than the 3-phase GSCM. From Figure 10(b), 4 case studies gave very much similar prediction results. In general, $(n+1)$ -phase models considering the multilayer properties of rubber as inputs slightly increase the prediction accuracy, especially at intermediate frequencies. However, the underestimation of complex modulus at lower frequencies by these models remains unsolved.

5. Micromechanical models considering interparticle interactions

5.1. Possible explanations for the limitations of previous models

As explained earlier, MTM, SCM, GSCM and $(n+1)$ -phase model all failed to accurately predict the complex modulus of CRMB with high rubber contents at high temperatures (corresponding to low frequencies in the master curve). The reason is that none of these models explicitly account for the interparticle interactions at high concentrations. All the rubber particles, as equivalent inclusions, were taken as one phase for MTM, SCM and GSCM, and several disassociated phases for the $(n+1)$ -phase model. The particle's relative configuration (orientations and locations, etc.), and geometrical properties (e.g. size, shape, angularity, surface morphology, etc.) were not considered. Therefore, methods that can more properly address the interparticle interactions by considering the above factors should be investigated.

Generally, there are three stiffening mechanisms for particulate filled composites: volume-filling effect, physiochemical interaction and particle interaction. For the CRMB system in the current study, volume-filling reinforcement is the stiffening caused by the presence of rubber inclusion in the bitumen matrix where the stress/strain fields are disturbed because of the inconsistent mechanical properties of rubber and bitumen. Physiochemical stiffening is due to the swelling of rubber in

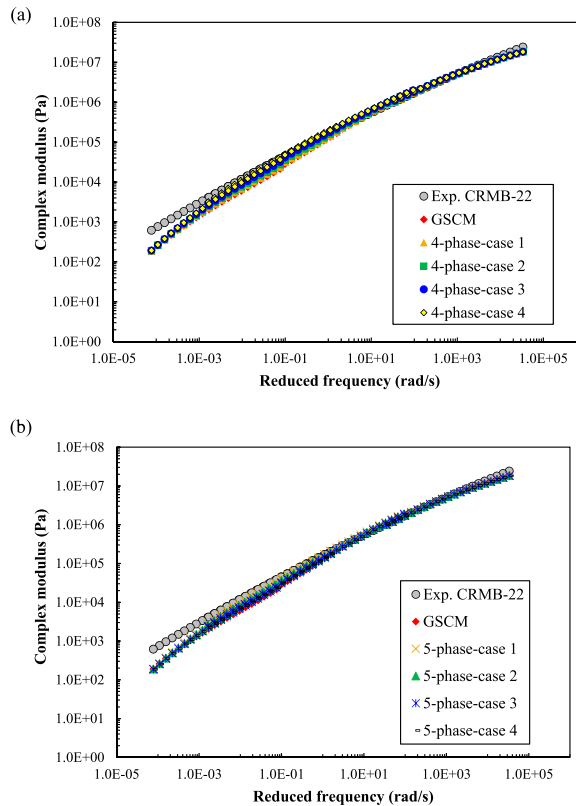


Figure 10. Complex modulus master curves of CRMB-22 predicted by (a) 4-phase model and (b) 5-phase model.

bitumen, which absorbs the bitumen components and increases the effective volume concentration of rubber inclusion. Interparticle interaction is a broad concept. The interparticle-interaction effect increases with increasing rubber content in bitumen, as rubber particles may come into contact and form a polymer network. The inability of accounting for the polymeric network because of particle interaction was shown by the underestimation of the complex modulus of previous models. In the previous models, the volume-filling reinforcement and the physiochemical effects were considered. The interparticle interactions were only partially considered without taking the particle's configuration and geometric properties into considerations. Therefore, new models, which bring in the effect of the particle's configuration, will be introduced in the following section.

5.2. J-C model

Previous models (i.e. MTM, SCM, GSCM and $(n+1)$ -phase model) were established based on the Eshelby's equivalent inclusion method (Yin et al., 2004), which means inclusions were treated as equivalent to each other and have no mutual impacts. Alternatively, they can also be called single-inclusion based models. To account for the particle-to-particle effect, Ju and Chen proposed a micromechanical model (J-C model) for two-phase composites by extending the equivalent inclusion scheme to a two-particle problem (Ju & Chen, 1994a). The strategy for this micromechanical framework is illustrated in Figure 11. Figure 11a shows a two-phase composite in which identical spheres with the radius a are randomly embedded in an infinite matrix material. Taking the central particle in Figure 11a as an example, its average strain $\bar{\epsilon}$ under the external far-field strain ϵ_0 comes from two parts: the perturbed

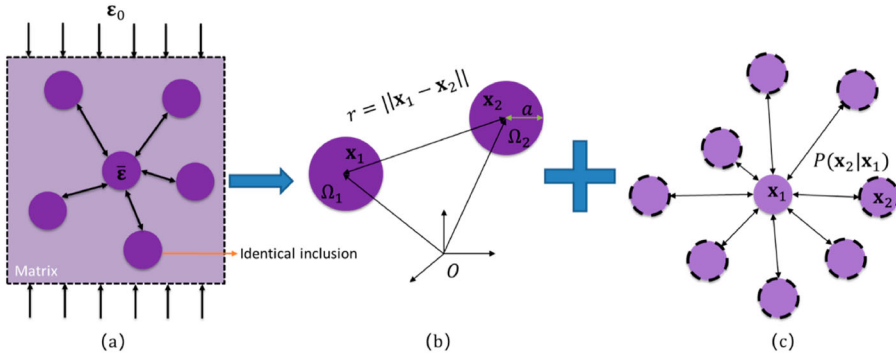


Figure 11. Schematic representation of the micromechanical framework of J-C model (a) two-phase composite with identical but randomly distributed inclusions; (b) pairwise particle interaction; (c) probabilistic pairwise particle interaction.

strain due to the mechanical mismatch between the particle and the matrix; and the perturbed strain due to the pairwise particle interaction between the central particle and other surrounding particles.

Therefore, the J-C model decomposes the multi-particle interaction problem into two steps. Firstly, approximate solutions for the pairwise particle interaction problem (Figure 11b) are derived. Then, a conditional probability function is introduced to account for the probabilistic pairwise interaction mechanism (Figure 11c). Combining the approximate solutions of the pairwise interaction problem and the governing ensemble-volume averaged field equations (Ju & Chen, 1994b), the effective elastic moduli of two-phase composites containing isotopically distributed identical spherical particles can be derived. The model was extended to predict the effective complex modulus by virtue of the elastic-viscoelastic corresponding principle.

5.2.1. Approximate solutions for pairwise particle interaction problem

In the micromechanical framework of the J-C model, two identical spherical rubber particles are embedded into a homogenous bitumen matrix, as shown in Figure 12. When subjected to a remote uniform strain ϵ_0 , the approximate solution for the pairwise particle interaction problem was obtained by subtracting the noninteracting solution from the distributed eigenstrain (Ju & Chen, 1994a) as in Equation (5).

$$\mathbf{d}^* = \mathbf{e}^*(\mathbf{x}) - \mathbf{e}_0^* \quad (5)$$

where $\mathbf{e}^*(\mathbf{x})$ is the distributed eigenstrain at \mathbf{x} within the domain Ω . $\Omega = 4\pi a^3/3$ is the volume of the spherical particle. It is only nonzero within the particle domain. \mathbf{e}_0^* is the “noninteracting” solution for eigenstrain. Accurate to the order of $O(\rho^8)$, the average of the second-order pairwise interaction tensor \mathbf{d}^* , which is $\bar{\mathbf{d}}^* = \frac{1}{\Omega} \int_{\Omega} (\mathbf{e}^*(\mathbf{x}) - \mathbf{e}_0^*) d\mathbf{x}$, can be approximately expressed by the following equation (Ju & Chen, 1994a)

$$\bar{\mathbf{d}}^* = -[\mathbf{K}^{-1} \cdot (\rho^3 \mathbf{H}_1 + 2\rho^5 \mathbf{H}_2)] : \mathbf{e}_0^* - \rho^6 [\mathbf{L} \cdot \mathbf{H}_1] : \mathbf{e}_0^* + O(\rho^8) \quad (6)$$

where $\rho = a/r$; $r = \|\mathbf{x}_1 - \mathbf{x}_2\|$; and

$$K_{ijkl} = F_{ijkl}(0, 0, 0, 0, \alpha, \beta) \quad (7)$$

$$L_{ijkl} = \frac{5}{4\beta^2} F_{ijkl} \left(-15, 3v_b, \frac{6\alpha(1-2v_b)}{3\alpha+2\beta}, \frac{6\alpha(1+v_b)}{3\alpha+2\beta}, -\frac{2\alpha(2-v_b)}{3\alpha+2\beta}, 1-2v_b \right) \quad (8)$$

$$H_{1ijkl} = 5F_{ijkl}(-15, 3v_b, 3, 3-6v_b, -1+2v_b, 1-2v_b) \quad (9)$$

$$H_{2ijkl} = 3F_{ijkl}(35, -5, -5, -5, 1, 1) \quad (10)$$

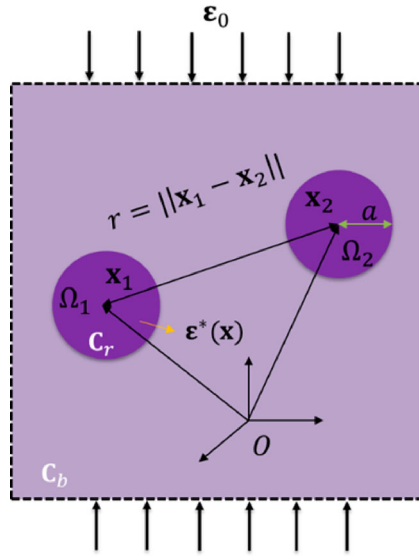


Figure 12. Schematic illustration for pairwise particle interaction problem.

in which the components of the fourth-order tensor \mathbf{F} , which depends on its arguments B_m ($m = 1-6$), are defined as

$$\begin{aligned}
 F_{ijkl}(B_m) = & B_1 n'_i n'_j n'_k n'_l + B_2 (\delta_{ik} n'_j n'_l + \delta_{il} n'_j n'_k + \delta_{jk} n'_i n'_l + \delta_{jl} n'_i n'_k) \\
 & + B_3 \delta_{ij} n'_k n'_l + B_4 \delta_{kl} n'_i n'_j + B_5 \delta_{ij} \delta_{kl} + B_6 (\delta_{ik} \delta_{jl} + \delta_{il} \delta_{jk})
 \end{aligned}
 \tag{11}$$

with the normal vector $\mathbf{n}' = \mathbf{r}/r$ and δ_{ij} as the Kronecker's delta. And

$$\alpha = 2(5v_b - 1) + 10(1 - v_b) \cdot \left(\frac{K_b}{K_r - K_b} - \frac{G_b}{G_r - G_b} \right)
 \tag{12}$$

$$\beta = 2(4 - 5v_b) + 15(1 - v_b) \cdot \frac{G_b}{G_r - G_b}
 \tag{13}$$

5.2.2. Ensemble-volume averaged eigenstrains

To obtain the ensemble-average solution of $\bar{\mathbf{d}}^*$ within the context of approximate pairwise particle interaction, Equation (6) needs to be integrated over all possible positions (\mathbf{x}_2) of the second particle for a given location of the first particle (\mathbf{x}_1) as shown below.

$$\langle \bar{\mathbf{d}}^* \rangle(\mathbf{x}_1) = \int_{V-\Omega_1} \bar{\mathbf{d}}^*(\mathbf{x}_1 - \mathbf{x}_2) P(\mathbf{x}_2|\mathbf{x}_1) d\mathbf{x}_2
 \tag{14}$$

where $\langle \bar{\mathbf{d}}^* \rangle$ is the ensemble-average solution and $P(\mathbf{x}_2|\mathbf{x}_1)$ is the conditional probability function. The two-point conditional probability function $P(\mathbf{x}_2|\mathbf{x}_1)$ basically describes the probability for finding the second particle centred at \mathbf{x}_2 when the first particle centres at \mathbf{x}_1 . It is related to the microstructure of the composite, or more specifically, to the particle volume fraction and the geometrical properties. Assuming that it is statistically isotropic and uniform, the probability function can be written in the

following form:

$$P(\mathbf{x}_2|\mathbf{x}_1) = \begin{cases} \frac{N}{V}g(r) & \text{when } r \geq 2a \\ 0 & \text{otherwise} \end{cases} \quad (15)$$

where N/V is the number of density particles in a composite, which is related to the particle volume fraction ϕ by Equation (13)

$$\frac{N}{V} = \frac{4\pi a^3}{3\phi} \quad (16)$$

r is the distance between the centres of two identical particles with a radius of a ; $g(r)$ is the radial distribution function (RDF). Substituting Equations (6) and (15) into Equation (14) leads to

$$\langle \bar{\mathbf{d}}^* \rangle = \frac{5\phi}{4\beta^2} Y(g) \mathbf{W} : \mathbf{e}_0^* \quad (17)$$

where

$$W_{ijkl} = \xi_1 \delta_{ij} \delta_{kl} + \xi_2 (\delta_{ik} \delta_{jl} + \delta_{il} \delta_{jk}) \quad (18)$$

$$\xi_1 = 12(13v_b - 14v_b^2) - \frac{96\alpha}{3\alpha + 2\beta} (1 - 2v_b)(1 + v_b) \quad (19)$$

$$\xi_2 = 6(25 - 34v_b + 22v_b^2) - \frac{36\alpha}{3\alpha + 2\beta} (1 - 2v_b)(1 + v_b) \quad (20)$$

$$Y(g) = \int_{2a}^{\infty} \frac{a^3}{r^4} g(r) dr = \int_0^{1/2} \rho^2 g(\rho) d\rho \quad (21)$$

It can be seen $Y(g)$ is related to the RDF and can be solved exactly with a given volume fraction ϕ . For a statistically uniform RDF ($g(\rho) = 1$), $Y(g)$ equals $1/24$. Further, the approximate ensemble-average eigenstrain tensor $\langle \bar{\mathbf{e}}^* \rangle$ can take the form:

$$\langle \bar{\mathbf{e}}^* \rangle = \mathbf{\Gamma} : \mathbf{e}_0^* \quad (22)$$

where the components of the isotropic tensor $\mathbf{\Gamma}$. are given by

$$\Gamma_{ijkl} = \gamma_1 \delta_{ij} \delta_{kl} + \gamma_2 (\delta_{ik} \delta_{jl} + \delta_{il} \delta_{jk}) \quad (23)$$

in which

$$\gamma_1 = \frac{5\phi}{4\beta^2} Y(g) \xi_1 \quad (24)$$

$$\gamma_2 = \frac{1}{2} + \frac{5\phi}{4\beta^2} Y(g) \xi_2 \quad (25)$$

5.2.3. Radial distribution function

RDF describes the density of surrounding matters as a function of the distance from a particular point in computational mechanics and statistical mechanics (Goodwin et al., 2006). For the classical fluid of hard (impenetrable) spheres, the Percus-Yevick (P-Y) function has been widely used to calculate the RDF and proved to be of great reliability. Many researchers have proposed different solutions for the P-Y function (Goodwin et al., 2006; Leonard et al., 1971; Perram, 1975; Wertheim, 1963).

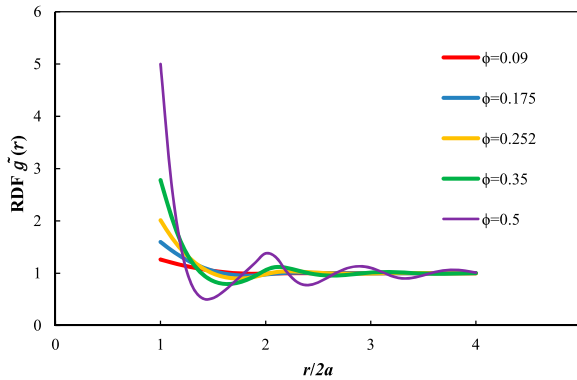


Figure 13. Radial distribution functions under different particle volume fractions.

In the current study, a more applicable and simple analytical solution was adopted by using the concept of normalised RDF as shown in Equation (26) (Zhang et al., 2019)

$$\tilde{g}(r) = \begin{cases} H(r - 1) \cdot \tilde{g}_1(r) + H(r - 2) \cdot \tilde{g}_2(r) + H(r - 3) \cdot \tilde{g}_3(r) & 1 < r/2a < 4 \\ 1 & r/2a \geq 4 \end{cases} \quad (26)$$

where $\tilde{g}(r)$ is the normalised RDF; $H(r - i)$ is the Heaviside function; $\tilde{g}_i(r)$ ($i = 1, 2, 3$) are the first three terms derived from the operation of Taylor expansion, which are functions of volume fractions. The detailed expressions for $\tilde{g}_i(r)$ ($i = 1, 2, 3$) can be found in (Zhang et al., 2019).

Figure 13 shows the RDFs for five different particle volume fractions. The effective volume fractions for CRMB-5, CRMB-10, CRMB-15, and CRMB-22 are 9.11%, 17.47%, 25.18%, and 35% respectively. The case $\phi = 0.5$ is plotted for comparison purposes. It is clear that the closer two particles (smaller $r/2a$) the more significant interaction (higher $\tilde{g}(r)$) can be observed. The $\tilde{g}(r)$ gradually reduced to 1 with the increase of particle distance. More importantly, with the increase of particle volume fraction, the RDF comes more fluctuating, indicating more significant interparticle interactions. For low volume fractions, the RDF tends to satisfy the uniform distribution $\tilde{g}(r) = 1$. The uniform distribution function assumes that the distribution of inclusions in the composite is isotropic and uniform in terms of statistical measurements, and thus $\tilde{g}(r)$ is identically equal to 1.

5.2.4. Effective viscoelastic moduli of CRMB system containing randomly dispersed identical spherical particles

For the two-phase composites containing randomly dispersed identical spherical particles, the average stress $\bar{\sigma}$, the average strain $\bar{\epsilon}$, the uniform remote strain ϵ_0 and the average particle eigenstrain $\bar{\epsilon}^*$ are related by the following equations:

$$\bar{\sigma} = \mathbf{C}_b : (\bar{\epsilon} - \phi \bar{\epsilon}^*) \quad (27)$$

$$\bar{\epsilon} = \epsilon_0 + \phi \mathbf{S} : \bar{\epsilon}^* \quad (28)$$

where \mathbf{S} is the Eshelby tensor and \mathbf{C}_b is the stiffness tensor of the matrix. Recalling the solution for the particle eigenstrain neglecting the interparticle interaction in the following equation:

$$\bar{\epsilon}^* = -(\mathbf{A} + \mathbf{S})^{-1} : \epsilon_0 \quad (29)$$

The average eigenstrain for the pairwise particle interaction problem can be derived as

$$\bar{\epsilon}^* = [\mathbf{\Gamma} \cdot (-\mathbf{A} - \mathbf{S} + \phi \mathbf{S} \cdot \mathbf{\Gamma})^{-1}] : \bar{\epsilon} \quad (30)$$

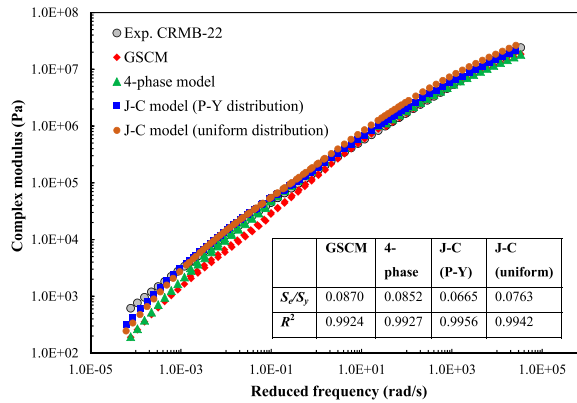


Figure 14. Comparison between complex modulus master curves of CRMB-22 predicted by different models.

Substituting Equation (30) into (27) yields the expression of effective stiffness tensor of the composite:

$$\mathbf{C}_c = \mathbf{C}_b \cdot [\mathbf{I} - \phi \mathbf{\Gamma} \cdot (-\mathbf{A} - \mathbf{S} + \phi \mathbf{S} \cdot \mathbf{\Gamma})^{-1}] \quad (31)$$

Accordingly, the effective bulk modulus K_c and the effective shear modulus G_c of the CRMB system with identical spherical rubber particles randomly dispersed in the bitumen matrix can be expressed in Equations (32) and (33).

$$K_c = K_b + \frac{30(1 - \nu_b)\phi(3\gamma_1 + 2\gamma_2)K_b}{3\alpha + 2\beta - 10(1 + \nu_b)\phi(3\gamma_1 + 2\gamma_2)} \quad (32)$$

$$G_c = G_b + \frac{30(1 - \nu_b)\phi\gamma_2 G_b}{\beta - 4(4 - 5\nu_b)\phi\gamma_2} \quad (33)$$

5.3. Prediction results from the J-C model

To further assess the validity of the J-C model, the predicted results were compared with the experimental data as well as the GSCM and 4-phase model (from the case with the best prediction) predictions. The material properties involved in the J-C model include the Poisson's ratios and the complex shear modulus master curves of the bitumen matrix phase and rubber inclusion phase. By substituting Equation (26) into Equation (21), $Y(g)$ was calculated as 0.064 when the effective volume fraction of rubber is 35% for CRMB-22. For comparison purpose, the uniform distribution of particles was also considered in the model in which $Y(g)$ equals 0.0417 (1/24). The complex moduli of each phase adopted the same experimental data as the other models. The bulk modulus was calculated based on the relationship between shear modulus and Poisson's ratio (Equation (34)) instead of experimental measurements.

$$K = \frac{2G(1 + \nu)}{3(1 - 2\nu)} \quad (34)$$

The complex modulus master curves of CRMB-22 predicted by different models are presented in Figure 14.

It can be seen that the J-C model considering pairwise particle interaction with a P-Y radial distribution function yields the best prediction accuracy among the models. The coefficient of determination reaches 0.9956. Besides, differences between the J-C model predicted results using the uniform distribution and P-Y distribution for particles can be observed. The predicted complex moduli from the uniform distribution are higher than that from the P-Y distribution at high frequencies but lower at low frequencies. This makes the master curve predicted from the uniform distribution deviate from

the experimental results in the whole frequency range. Using P-Y distribution for considering the particle's configuration, the J-C model predicted results are closer to the experimental data by decreasing the modulus at high frequencies and increasing the modulus at low frequencies. P-Y radial distribution function assumes the state of thermodynamic equilibrium distribution due to numerous particle collisions. It is quite suitable for the CRMB system which can be regarded as a colloidal suspension system. The J-C model not only remedies the underestimation of modulus in the low-frequency range by other models but also slightly increases the modulus at high frequencies. Therefore, the J-C model provides a substantial improvement for the prediction accuracy comparing to other models by properly addressing the interparticle interactions from the perspective of the particle's configuration.

6. Conclusions and recommendations

The study aims to improve the complex modulus prediction accuracy of CRMB by considering the interparticle interactions. Firstly, the $(n+1)$ -phase model was applied to the CRMB system by considering the multilayer properties of swollen rubber particles. Secondly, a new micromechanical scheme called the J-C model was used to account for the interparticle interaction issue. The main conclusions from this study can be drawn:

- The $(n+1)$ -phase models considering the multilayer properties of rubber as inputs slightly increase the prediction accuracy, especially at intermediate frequencies. However, the underestimation of complex modulus at lower frequencies by these models remains unsolved.
- The J-C model remedies the underestimation of modulus in the low-frequency range by other models and provides an overall improvement for the prediction accuracy comparing to other models by properly addressing the interparticle interactions from the perspective of particle's configuration.

For future work, it is expected to extend the models in this study to different types of CRMB with varying rubber size, rubber contents, bitumen sources, etc. Besides the particle's relative configuration considered in this study, the effects of geometrical properties (e.g. size, shape, angularity, surface morphology, etc.) on interparticle interaction can be further investigated.

Disclosure statement

No potential conflict of interest was reported by the author(s).

ORCID

Haopeng Wang  <http://orcid.org/0000-0002-5008-7322>

Athanasios Skarpas  <http://orcid.org/0000-0002-3478-8807>

Sandra Erkens  <http://orcid.org/0000-0002-2465-7643>

Zhen Leng  <http://orcid.org/0000-0002-7797-1134>

References

- Aragao, F. T. S., Kim, Y. R., Lee, J., & Allen, D. H. (2011). Micromechanical model for heterogeneous asphalt concrete mixtures subjected to fracture failure. *Journal of Materials in Civil Engineering*, 23(1), 30–38. [https://doi.org/10.1061/\(ASCE\)MT.1943-5533.0000004](https://doi.org/10.1061/(ASCE)MT.1943-5533.0000004)
- Aurangzeb, Q., Ozer, H., Al-Qadi, I. L., & Hilton, H. H. (2016). Viscoelastic and Poisson's ratio characterization of asphalt materials: Critical review and numerical simulations. *Materials and Structures*, 50(1), <https://doi.org/10.1617/s11527-016-0881-x>
- Buttler, W., Bozkurt, D., Al-Khateeb, G., & Waldhoff, A. (1999). Understanding asphalt mastic behavior through micromechanics. *Transportation Research Record: Journal of the Transportation Research Board*, 1681(1), 157–169. <https://doi.org/10.3141/1681-19>
- Caro, S., Masad, E., Bhasin, A., & Little, D. (2010). Micromechanical modeling of the influence of material properties on moisture-induced damage in asphalt mixtures. *Construction and Building Materials*, 24(7), 1184–1192. <https://doi.org/10.1016/j.conbuildmat.2009.12.022>

- Ceylan, H., Schwartz, C. W., Kim, S., & Gopalakrishnan, K. (2009). Accuracy of predictive models for dynamic modulus of hot-mix asphalt. *Journal of Materials in Civil Engineering*, 21(6), 286–293. [https://doi.org/10.1061/\(Asce\)0899-1561\(2009\)21:6\(286\)](https://doi.org/10.1061/(Asce)0899-1561(2009)21:6(286))
- Charalambakis, N. (2010). Homogenization techniques and micromechanics. A survey and perspectives. *Applied Mechanics Reviews*, 63(3), doi:Artn 03080310.1115/1.4001911
- Goodwin, S. P., Boughey, J. D., & Heritage, J. R. (2006). Calculation of the hard sphere radial distribution function. *Molecular Physics*, 75(4), 917–923. <https://doi.org/10.1080/00268979200100691>
- Herve, E., & Zaoui, A. (1993). N-layered inclusion-based micromechanical modelling. *International Journal of Engineering Science*, 31(1), 1–10. [https://doi.org/10.1016/0020-7225\(93\)90059-4](https://doi.org/10.1016/0020-7225(93)90059-4)
- Ju, J. W., & Chen, T. M. (1994a). Effective elastic moduli of two-phase composites containing randomly dispersed spherical inhomogeneities. *Acta Mechanica*, 103(1–4), 123–144. <https://doi.org/10.1007/BF01180222>
- Ju, J. W., & Chen, T. M. (1994b). Micromechanics and effective moduli of elastic composites containing randomly dispersed ellipsoidal inhomogeneities. *Acta Mechanica*, 103(1–4), 103–121. <https://doi.org/10.1007/Bf01180221>
- Leonard, P. J., Henderson, D., & Barker, J. A. (1971). Calculation of the radial distribution function of hard-sphere mixtures in the Percus-Yevick approximation. *Molecular Physics*, 21(1), 107–111. <https://doi.org/10.1080/00268977100101221>
- Leon L. Mishnaevsky, J., & Schmauder, S. (2001). Continuum mesomechanical finite element modeling in materials development: A state-of-the-Art review. *Applied Mechanics Reviews*, 54(1), 49–67. <https://doi.org/10.1115/1.3097288>
- Medina, J. R., & Underwood, B. S. (2017). Micromechanical shear modulus modeling of activated crumb rubber modified asphalt cements. *Construction and Building Materials*, 150, 56–65. <https://doi.org/10.1016/j.conbuildmat.2017.05.208>
- Nanjegowda, V. H., & Biligiri, K. P. (2020). Recyclability of rubber in asphalt roadway systems: A review of applied research and advancement in technology. *Resources, Conservation and Recycling*, 155, 104655. <https://doi.org/10.1016/j.resconrec.2019.104655>
- Perram, J. W. (1975). Hard sphere correlation functions in the Percus-Yevick approximation. *Molecular Physics*, 30(5), 1505–1509. <https://doi.org/10.1080/00268977500103021>
- Sadd, M. H., Dai, Q. L., Parameswaran, V., & Shukla, A. (2004). Microstructural simulation of asphalt materials: Modeling and experimental studies. *Journal of Materials in Civil Engineering*, 16(2), 107–115. [https://doi.org/10.1061/\(Asce\)0899-1561\(2004\)16:2\(107\)](https://doi.org/10.1061/(Asce)0899-1561(2004)16:2(107))
- Shen, J., Amirkhani, S., Xiao, F., & Tang, B. (2009a). Influence of surface area and size of crumb rubber on high temperature properties of crumb rubber modified binders. *Construction and Building Materials*, 23(1), 304–310. <https://doi.org/10.1016/j.conbuildmat.2007.12.005>
- Shen, J., Amirkhani, S., Xiao, F., & Tang, B. (2009b). Surface area of crumb rubber modifier and its influence on high-temperature viscosity of CRM binders. *International Journal of Pavement Engineering*, 10(5), 375–381. <https://doi.org/10.1080/10298430802342757>
- Shu, X., & Huang, B. (2008). Micromechanics-based dynamic modulus prediction of polymeric asphalt concrete mixtures. *Composites Part B: Engineering*, 39(4), 704–713. <https://doi.org/10.1016/j.compositesb.2007.05.003>
- Wang, H., Apostolidis, P., Zhu, J., Liu, X., Skarpas, A., & Erkens, S. (2020). The role of thermodynamics and kinetics in rubber-bitumen systems: A theoretical overview. *International Journal of Pavement Engineering*, 1–16. <https://doi.org/10.1080/10298436.2020.1724289>
- Wang, H., Liu, X., Apostolidis, P., Erkens, S., & Scarpas, T. (2019). Numerical investigation of rubber swelling in bitumen. *Construction and Building Materials*, 214, 506–515. <https://doi.org/10.1016/j.conbuildmat.2019.04.144>
- Wang, H., Liu, X., Apostolidis, P., Erkens, S., & Scarpas, A. (2020). Experimental investigation of rubber swelling in bitumen. *Transportation Research Record: Journal of the Transportation Research Board*, 2674(2), 203–212. <https://doi.org/10.1177/0361198120906423>
- Wang, H., Liu, X., Apostolidis, P., & Scarpas, T. (2018). Rheological behavior and its chemical interpretation of crumb rubber modified asphalt containing warm-Mix additives. *Transportation Research Record: Journal of the Transportation Research Board*, 2672(28), 337–348. <https://doi.org/10.1177/0361198118781376>
- Wang, H., Liu, X., Zhang, H., Apostolidis, P., Erkens, S., & Skarpas, A. (2020). Micromechanical modelling of complex shear modulus of crumb rubber modified bitumen. *Materials & Design*, 188. <https://doi.org/10.1016/j.matdes.2019.108467>
- Wang, H., Liu, X., Zhang, H., Apostolidis, P., Scarpas, T., & Erkens, S. (2020). Asphalt-rubber interaction and performance evaluation of rubberised asphalt binders containing non-foaming warm-mix additives. *Road Materials and Pavement Design*, 21(6), 1612–1633. <https://doi.org/10.1080/14680629.2018.1561380>
- Wertheim, M. S. (1963). Exact solution of the Percus-Yevick integral equation for hard spheres. *Physical Review Letters*, 10(8), 321–323. <https://doi.org/10.1103/PhysRevLett.10.321>
- Willis, J. R., Turner, P., Plemmons, C., Rodezno, C., Rosenmayer, T., Daranga, C., & Carlson, D. (2013). Effect of rubber characteristics on asphalt binder properties. *Road Materials and Pavement Design*, 14(sup2), 214–230. <https://doi.org/10.1080/14680629.2013.812845>
- Yin, H. M., Buttlar, W. G., Paulino, G. H., & Benedetto, H. D. (2008). Assessment of existing micro-mechanical models for asphalt mastics considering viscoelastic effects. *Road Materials and Pavement Design*, 9(1), 31–57. <https://doi.org/10.1080/14680629.2008.9690106>
- Yin, H. M., Sun, L. Z., & Paulino, G. H. (2004). Micromechanics-based elastic model for functionally graded materials with particle interactions. *Acta Materialia*, 52(12), 3535–3543. <https://doi.org/10.1016/j.actamat.2004.04.007>

- Zhang, H., Anupam, K., Scarpas, T., Kasbergen, C., Erkens, S., & Al Khateeb, L. (2020). Continuum-based micromechanical models for asphalt materials: Current practices & beyond. *Construction and Building Materials*, 260. 119675. <https://doi.org/10.1016/j.conbuildmat.2020.119675>
- Zhang, H., Anupam, K., Scarpas, A., & Kasbergen, C. (2018). Comparison of different micromechanical models for predicting the effective properties of open graded mixes. *Transportation Research Record*, 2672(28), 404–415. <https://doi.org/10.1177/0361198118794713>.
- Zhang, J., Fan, Z., Wang, H., Sun, W., Pei, J., & Wang, D. (2019). Prediction of dynamic modulus of asphalt mixture using micromechanical method with radial distribution functions. *Materials and Structures*, 52(2). <https://doi.org/10.1617/s11527-019-1348-7>